Published in final edited form as:
J Aerosol Sci. 2012 September ; 51: 66–80. doi:10.1016/j.jaerosci.2012.04.002.

Production of Inhalable Submicrometer Aerosols from Conventional Mesh Nebulizers for Improved Respiratory Drug Delivery

P. Worth Longest[1,2,*], **Benjamin M. Spence**[1], **Landon T. Holbrook**[1], **Karla M. Mossi**[1], **Yoen-Ju Son**[2], and **Michael Hindle**[2]

[1]Department of Mechanical Engineering Virginia Commonwealth University, Richmond, VA

[2]Department of Pharmaceutics Virginia Commonwealth University, Richmond, VA

Abstract

Submicrometer and nanoparticle aerosols may significantly improve the delivery efficiency, dissolution characteristics, and bioavailability of inhaled pharmaceuticals. The objective of this study was to explore the formation of submicrometer and nanometer aerosols from mesh nebulizers suitable for respiratory drug delivery using experiments and computational fluid dynamics (CFD) modeling. Mesh nebulizers were coupled with add-on devices to promote aerosol drying and the formation of submicrometer particles, as well as to control the inhaled aerosol temperature and relative humidity. Cascade impaction experiments were used to determine the initial mass median aerodynamic diameters of 0.1% albuterol aerosols produced by the AeroNeb commercial (4.69 μm) and lab (3.90 μm) nebulizers and to validate the CFD model in terms of droplet evaporation. Through an appropriate selection of flow rates, nebulizers, and model drug concentrations, submicrometer and nanometer aerosols could be formed with the three devices considered. Based on CFD simulations, a wire heated design was shown to overheat the airstream producing unsafe conditions for inhalation if the aerosol was not uniformly distributed in the tube cross-section or if the nebulizer stopped producing droplets. In comparison, a counter-flow heated design provided sufficient thermal energy to produce submicrometer particles, but also automatically limited the maximum aerosol outlet temperature based on the physics of heat transfer. With the counter-flow design, submicrometer aerosols were produced at flow rates of 5, 15, and 30 LPM, which may be suitable for various forms of oral and nasal aerosol delivery. Thermodynamic conditions of the aerosol stream exiting the counter-flow design were found be in a range of 21-45 °C with relative humidity greater than 40% in some cases, which was considered safe for direct inhalation and advantageous for condensational growth delivery.

Keywords

Respiratory drug delivery; nanoaerosols; droplet evaporation; CFD simulation of droplet evaporation; two-way coupled heat and mass transfer; hygroscopic droplets; cascade impaction testing

[*](Corresponding author): Dr. P. Worth Longest, PhD, Virginia Commonwealth University, 401 West Main Street, P.O. Box 843015, Richmond, VA 23284-3015, Phone: (804)-827-7023, Fax: (804)-827-7030, pwlongest@vcu.edu.

1. Introduction

The use of submicrometer and nanometer aerosols for respiratory drug delivery is reported to have a number of advantages compared with conventional systems. Submicrometer and nanometer particles provide better dissolution of poorly soluble drugs (El-Gendy et al., 2009; Yang et al., 2008) and reduce clearance by both macrophages (Azarmi et al., 2008) and mucus entanglement (Lai et al., 2009) compared with conventional micrometer particles. Submicrometer and nanoparticle aerosols in the size range of 40 - 1000 nm are also known to have very low deposition fractions in the oral and nasal extrathoracic airways, thereby dramatically reducing depositional losses and associated side effects compared with conventional-sized aerosols (Cheng et al., 1996; Xi and Longest 2007; Xi and Longest 2008a; Xi and Longest 2008b). The increased deposition of nanoaerosols in the alveolar airways due to Brownian motion, which can be used to deliver aerosolized medicines, has been reported for some time (Asgharian and Price 2007; Dandekar et al., 2010; Finlay 2001; Jaques and Kim 2000; Martonen 1993). However, practical implementation of this approach for effective respiratory drug delivery may be limited by access to a convenient source of inhalable submicrometer or nanoscale aerosols.

Condensational growth of submicrometer aerosols is a newly proposed approach to significantly improve the delivery of pharmaceutical aerosols to the lungs (Hindle and Longest 2010; Longest and Hindle 2011; Longest et al., 2010). In this method, submicrometer aerosols are formed and delivered to either the nasal or oral extrathoracic airways. The small aerosol size and low inertia of the droplets results in negligible (~1%) extrathoracic deposition (Hindle and Longest 2010). Two approaches are then available to increase particle size and ensure full lung retention of the aerosol. The enhanced condensational growth (ECG) approach delivers the initially submicrometer aerosol with a stream of air saturated with water vapor at a temperature a few degrees above airway conditions. Cooling of the airstream within the airways causes condensation onto the droplets and size increase to the micrometer range (Hindle and Longest 2010; Longest et al., 2011; Tian et al., 2011). In comparison with ECG, the enhanced excipient growth (EEG) approach implements the delivery of combination drug and hygroscopic excipient submicrometer droplets or particles without an inhaled saturated airstream. Near saturated conditions within the lungs are used to foster size increase of the hygroscopic droplets and ensure deposition of the aerosol (Hindle and Longest 2012; Longest and Hindle 2011; Longest and Hindle 2012).

A number of methods are currently available for the production of submicrometer and nanometer pharmaceutical aerosols. Electro-hydrodynamic atomization or electrospraying can effectively generate highly monodisperse droplets of micrometer or submicrometer size for pharmaceutical applications (Yurteri et al., 2010). However, liquid flow rates are very low compared with conventional medical aerosol delivery systems and the resulting highly charged droplets require neutralization for effective delivery to the lungs (Ijsebaert et al., 2001). Nanoscale pharmaceutical particles have been developed using wet-milling and solvent-based processes (Chan and Kwok 2011; Chen et al., 2002; Couvreur et al., 1995), which typically require the addition of large amounts of surfactants or other compounds to control aggregation. Similarly, spray drying can be used to form submicrometer particles (Chan and Kwok 2011). While these formation techniques are effective, creating a nanoaerosol for delivery to humans requires re-dispersing the particles, which can be challenging due to significant cohesive forces. Hindle et al. (2004) reported the formation of nanoparticle cromolyn sodium and insulin aerosols for direct inhalation using a capillary aerosol generator (CAG), which is not commercially available. The CAG was employed to effectively create submicrometer aerosols in the studies of Longest and Hindle (2011; 2012) for condensational growth testing. Other studies on condensational growth for respiratory

drug delivery have employed a commercial nebulizer, the small particle aerosol generator (SPAG) with an increased drying gas flow rate to form the submicrometer aerosol (Hindle and Longest 2010; Longest et al., 2010). A disadvantage of the SPAG is that temperatures of the aerosol were relatively low due to droplet evaporation, which may cause uncomfortable nasal delivery at high flow rates.

Mesh nebulizers have been available for respiratory drug delivery for over a decade and can now be considered a conventional technology. These devices form an aerosol suitable for respiratory drug delivery by vibrating a plate with micro-orifices against a liquid supply using either piezoelectric or magnetic actuation (Dhand 2002). Compared with conventional jet nebulizers, mesh devices have the advantages of providing intermittent aerosol delivery that can be coordinated with inhalation, similar liquid and drug delivery rates, and a more monodisperse aerosol (Dhand 2008; Pitance et al., 2010; Skaria and Smaldone 2010). Recently, mesh nebulizers have been coupled with breath-activation technology to significantly improve the fraction of nebulized liquid delivered to the patient and deposited in the lungs despite their relatively large particle size distribution. For oral delivery with breath-activation, mesh devices are reported to deliver approximately 60-70% of the nebulized volume to the lungs (Nikander et al., 2010). Delivering the aerosol through connective tubing and patient interfaces during invasive and non-invasive mechanical ventilation presents a significant challenge compared with direct oral inhalation (Dhand 2007). Ari et al. (2011) reported 2-10% aerosol delivery at the outlet of a nasal cannula for an infant using a conventional mesh nebulizer during high flow therapy. Abdelrahim et al. (2011) reported low lung bioavailability for both jet and mesh nebulized drugs delivered during non-invasive ventilation. Further improvements in aerosol delivery during mechanical ventilation will likely require reducing the aerodynamic size of the aerosol.

In this study, it is proposed that mesh nebulizers may provide a convenient source of submicrometer aerosols suitable for respiratory drug delivery, with a focus on generating aerosols for ECG and EEG approaches. Current mesh nebulizers typically produce aerosols in the size range of 4-6 μm (Kuhli et al., 2009). It is not likely possible to reduce the size of jet nebulizer droplets to the submicrometer and nanometer ranges by decreasing the aperture sizes of the vibrating plate due to surface interactions with the liquid (Zhang et al., 2007a), and doing so would significantly increase delivery times. Instead, add-on devices will be coupled to available mesh nebulizers to facilitate size reduction by drying with and without the inclusion of heat. Current devices for controlling the temperature of respiratory gasses include wire heaters and water jacketed heating. Wire heating systems contain a resistance heated wire in the gas delivery lines (Rea et al., 2010). Water jacketed heating surrounds the gas delivery line with a second line of temperature-controlled water (Guerrero et al., 2003). Wire heating is simpler, but provides less temperature control. The water jacketing approach adds the complexity of a water source, pump, and temperature regulator to the system. Neither approach has previously been used to foster the formation of submicrometer aerosols for direct inhalation.

The objective of this study is to explore the formation of submicrometer and nanometer aerosols from mesh nebulizers suitable for respiratory drug delivery using both *in vitro* experiments and computational fluid dynamics (CFD) modeling. Conventional mesh nebulizers are coupled with add-on devices to promote aerosol drying and the formation of submicrometer particles, as well as to control the inhaled temperature and relative humidity for improved performance during ECG and EEG delivery. All devices include a custom radial mixer that combines dry ambient gas with the aerosol and a 1 meter section of tubing leading to the patient mouthpiece. Three variations of the 1 m tube are considered, which are an insulated tube, a tube with external wire heating, and a jacketed tube heated with co-flow air. The systems are evaluated in terms of their ability to produce a submicrometer aerosol

using temperatures and flow rates that are safe and comfortable for direct inhalation. Based on the focus of generating submicrometer particles for ECG and EEG delivery, achieving outlet temperatures in predetermined ranges will also be considered.

2. Methods

2.1. Devices and Boundary Conditions

To form a temperature and humidity controlled submicrometer aerosol, two nebulizers were combined with three potential add-on devices. The nebulizers were the commercial version of the Aeroneb Pro and the Aeroneb Lab (both from Aerogen Limited, Galway, Ireland). The lab version reportedly has a smaller mass median aerodynamic diameter (MMAD) than the commercial nebulizer at the expense of a slower liquid delivery rate, which was verified experimentally (Table 1). Dry air from a house compressed-air line was filtered and combined with the nebulized aerosol using a custom fabricated radial mixer or diluter (Fig. 1a). The diluted aerosol stream exited the mixer and entered a 1 m segment of corrugated ventilator tubing (T10040INVV22; GlobalMed Inc., Ontario, Canada) with a diameter of 12 mm. Conditions of the 1 m length of tubing differentiate the three add-on devices considered. In the first system, no heat was added to the delivery tubing and evaporation was driven entirely by the vapor capacity of the dry inlet air (Fig. 1b). Due to the relatively low thermal conductivity of the plastic tubing and the presence of surrounding ambient air, the unheated system was considered to be insulated.

In the second system, an external heating wire was wound around the 12 mm delivery tubing, which provides a nearly uniform heat flux and is referred to as the wire heated case (also Fig. 1b). In the experimental version of this design, a layer of heat-shrink tubing was used to secure the external heating wire and insulate the system.

To simplify existing water jacketed delivery systems used with ventilation gases, a new air jacketed delivery system was developed (Fig. 1c). The inner line that carries the aerosol had a diameter of 12 mm and the outer jacketing line was standard 22 mm ventilator tubing (CORR-A-FLEX II; Hudson RCI, Research Triangle Park, NC). The heating gas was implemented to flow in the opposite direction of the aerosol stream forming a counter-flow heat exchanger, which is known to optimize heat transfer efficiency (Kays and Crawford 1993). In all cases, the heating air was maintained at 80 LPM with an input temperature of 42 °C at the counter-flow input port using an inline resistance heater (OMEGALUX AHP-5052; Omega Engineering Inc., Stamford, CT) and voltage regulator.

For consistency among the systems, the tubing was considered to be in a straight configuration. However, tube curvature will modify convective heat and mass transfer at the air-wall interfaces thereby influencing the evaporation of the aerosol and the exiting thermodynamic conditions. To assess the effects of tube curvature on outlet conditions, a second configuration was considered with curvature on 2 axes and a total length of 1 m (Fig. 1d).

It is envisioned that these devices will be used to deliver submicrometer aerosols in combination with ECG or EEG approaches during non-invasive ventilation and conventional oral delivery. Non-invasive ventilation (NIV) has a variety of forms including low flow and high flow oxygen delivery through nasal cannulas. Gas delivery flow rates of 5 and 15 LPM are representative of low flow cannula delivery to both nostrils or high flow delivery to one nasal passage (Longest et al., 2011), respectively. For oral aerosol delivery, 30 LPM is a representative and frequently used flow rate for nebulizers. While other variations are possible, flow rates of 5, 15, and 30 LPM are considered consistent with low

flow nasal cannula, high flow nasal cannula, and oral delivery of the aerosol to adults in this study.

In the CFD model, the most appropriate boundary conditions were sought to represent each design. For the case without heating, the relatively high thermal resistance of the delivery tubing, and the fact that the tubing was surrounded by ambient air, resulted in the assumption of an insulated wall boundary condition. Considering the wall heated design, an estimate of the input heat at the interface between the tube surface and air was required. The minimum amount of heat needed to both warm the gas mixture (air and water vapor) from inlet conditions (21 °C) to body temperature (37 °C) and completely evaporate the aerosol was calculated as

$$\dot{q} = \dot{m}_{\text{gas}} (h_{37} - h_{21}) + \dot{m}_{\text{liquid}} h_{fg} \quad (1)$$

where m is the inlet mass flow rate of gas and liquid (Table 1), h is the enthalpy per unit mass of the gas mixture at inlet and outlet temperatures, and h_{fg} is the heat of vaporization of the liquid. Enthalpy associated with heating the liquid droplets was neglected due to its being a factor of 2 - 20 times smaller than the gas enthalpy and at least an order of magnitude smaller than the heat required to vaporize the liquid. Heat transfer conditions within the tube then determine if the aerosol is fully evaporated and the air is uniformly warmed to the desired temperature. In order to minimize the potential for overheating the airstream, the minimum required input heat calculated by Eq. (1) was used to determine the uniform heat flux through the wall of the 1 m tube. Due to the high heat of vaporization of water, the input heat required to evaporate the water is up to 11 times the heat needed to raise the air temperature. The potential for overheating the airstream with the wall heated design will be considered later in this study.

For the counter-flow heated system, the interface between the heating gas and aerosol stream was assumed to be a conducting boundary. This boundary is described by convection at the two air-wall interface surfaces with conduction occurring through the 1 mm thick wall. The thermal properties of the plastic wall were assumed to be density $\rho = 1100$ kg/m^3, specific heat Cp = 2010 J/kg-K, and thermal conductivity k = 0.13 W/m-K (Green 1997). The outer wall of the counter-flow system was assumed to be insulated due to the presence of surrounding ambient air. In all cases, steady state conditions were assumed.

Mass flux of water vapor on the surface of the tubes is difficult to capture with a CFD model. Because water vapor in the system only comes from evaporating droplets, the maximum relative humidity (RH) is 100%. For an insulated system, there is a startup period over which some saturated water vapor will adhere to the device walls. This process will occur until the walls are covered with a layer of water. Thereafter, zero mass flux of water will occur for insulated conditions. However, surface droplet formation (beading) and heat transfer during condensation and evaporation will complicate this process. The best boundary condition for the insulated system then depends on the operating time. In this study experiments were conducted to size the aerosol over a short time period (30 - 50 s). However, operation of the aerosol system based on mesh nebulizer output rate is approximately 10 to 20 minutes to deliver a typical nebulizer liquid volume of 4 ml. As a result, comparisons with the experimental data in an insulated system assume zero mass wall concentration. In contrast, evaluations of system performance at steady state conditions for assessing device performance assume zero wall mass flux. All heated systems also assume zero wall mass flux of water vapor.

2.2. Experimental Methods

Experiments were used to determine the initial size of the aerosol, predict aerosol size when exposed to ambient conditions, and verify CFD results for the counter-flow system with both nebulizers. Additional experiments were conducted to determine the liquid mass flow rates from the lab and commercial Aeroneb devices. In all cases, the commercial and lab versions of the Aeroneb were used with an aqueous-based solution containing 0.1% w/v albuterol (as sulfate (AS)). Previous experimental measurements have indicated that AS is mildly hygroscopic with a van't Hoff factor of 2.1 and a hygroscopic parameter of 4.9 (Longest and Hindle 2011). For comparison, NaCl has a hygroscopic parameter of 77.9, as defined by Longest and Hindle (2011).

The experimental sizing apparatus consisted of a radial mixer similar to Fig. 1a, but with a 22 mm diameter outlet, a 25 cm section of 22 mm diameter tubing, and a horizontally positioned Andersen cascade impactor (ACI, Graseby-Andersen Inc, Smyrna, GA) maintained at ambient temperature and humidity. A minimum of 4 replicas were performed of each sizing experiment. Evaporation is known to affect the size of nebulized aerosol after formation (Abdelrahim and Chrystyn 2009; Kuhli et al., 2009). To determine the initial size distributions, aerosols from the commercial and lab nebulizers were evaluated using inlet air at 21 °C and 99% RH drawn from an environmental cabinet (Espec, Hudsonville, MI) at 30 LPM. Due to the absence of evaporation with 99% RH, initial sizes should not change for different sampling flow rates.

The particle size distribution of the aerosols generated from both nebulizers using ambient room air (55% RH) drawn into the mixer was evaluated to investigate the evaporation of water from the aerosol droplets. Aerosol sizes using room air at both 15 and 30 LPM sampling flow rates were evaluated for both nebulizers. For the case of 15 LPM sampling, makeup air was supplied at the impactor inlet at saturated RH conditions to prevent further evaporation of the aerosol and to ensure the impactor was operating at 30 LPM.

In addition, an experimental verification study was performed of the CFD results for the jacketed line case with conditions predicted to result in full evaporation or near full evaporation of the aerosol. For these verification experiments, the mixer and delivery tube configuration shown in Figs. 1a and c were prototyped and considered with inlet flow rates and temperatures matching the CFD conditions. The experimental system was allowed to reach steady state over a period of approximately 5 minutes before sampling the output aerosol size. Due to the small size of the aerosol after drying, a 10 stage MOUDI operated at 30 ± 2 LPM (MSP Corp, Shoreview, MN), which allowed size fractionation between 50 nm and 10 μm, was implemented for cascade impaction sizing.

For determining particle size distributions, washings using appropriate volumes of deionized water (5-25 ml) were collected from the impaction plates to evaluate the drug deposition following aerosol generation. The solutions were then assayed using validated HPLC-UV methods for AS. The mass of AS on each impaction plate was determined and used to calculate the aerodynamic particle size distributions of the drug. Aerosol particle size distributions were reported as mass distribution recovered from the impactor. The mass median aerodynamic diameter (MMAD) was defined as the particle size at the 50th percentile on a cumulative percent mass undersize distribution (D50) using linear interpolation. At least four replicates of each experiment were performed.

2.3. CFD Model and Numerical Methods

The transport dynamics of the dryer systems include laminar, transient, and turbulent flows, multiple species (air and water vapor), multiple phases, aerosol size change, strong two-way coupling between the phases, and interactions with the walls. Reynolds numbers range

between 217 and 3,449 within the mixer and delivery tube for the aerosol stream flow rates considered, and the average Reynolds number in the counter-flow line is 8,667. Longest and Hindle (2010) recently described CFD methods for simulating aerosol condensation and evaporation with multicomponent droplets including two-way coupling. These methods were largely employed in the current study. For completeness, these CFD methods are briefly reviewed below with differences from the study of Longest and Hindle (2010) highlighted.

To model laminar through turbulent conditions, the low Reynolds number (LRN) k-ω approach was selected based on its effectiveness and successful use in previous studies in simulating both aerosol size change and deposition (Longest and Hindle 2009; Longest and Hindle 2010; Longest and Hindle 2012; Longest et al., 2007; Longest and Vinchurkar 2007). The related governing equations for mass and momentum transport along with turbulence variables are available in Wilcox (1998) and Longest and Xi (2008). Coupled heat and mass convective-diffusive equations for turbulent flow were previously reported by Longest and Hindle (2010). These expressions include source terms to account for the exchange of heat and water vapor mass between the phases during droplet evaporation. Particle tracking was performed using a Lagrangian approach including terms for drag, gravity, and Brownian motion (Longest and Xi 2007). Due to low expected levels of turbulence in the aerosol delivery tubes, turbulent dispersion was neglected in this study. The quality of this assumption and its effect on the outlet particle or droplet diameters will be assessed based on comparisons with experimental results. Droplet evaporation and condensation models along with expressions for droplet properties, including hygroscopic effects for multiple solutes, were previously reported by Longest and Hindle (2010).

The commercial CFD package Fluent 12 (ANSYS, Inc.) was employed to solve the governing equations in all cases considered. User-supplied Fortran and C programs were used for the calculation of initial flow and droplet profiles, hygroscopic droplet evaporation, near-wall particle interpolation (Longest and Xi 2007), Brownian motion (Longest and Xi 2007), as well as heat and mass sources and sinks during two-way coupling. CFD best practices were employed including the use of second order or higher discretization, hexahedral grids (Vinchurkar and Longest 2008), and double precision calculations. Grid converged results based on negligible change in the velocity and temperature fields (< 1%) as well as negligible differences in the outlet droplet size (< 5%) were established for a mesh consisting of 457,000 control volumes for the counter-flow heated case and 195,000 control volumes for the insulated and wire heated systems.

All CFD results were computed for steady state conditions. In the initial RH field of either 0 or 55% with one-way coupling, droplets evaporate to dry particles very near the inlet. However, it is the two-way coupling between the discrete and continuous phases that ultimately limits the final size of the aerosol. As a result, the system was found to be extremely sensitive to two-way coupling effects and a very small under relaxation factor (URF) on the mass and energy source terms was required. For converged solutions, URFs on the source terms ranged from 0.08 to 0.05 with 120 iterations per discrete phase update. It was found that the number of required discrete phase updates for a converged solution could be determined using the expression

$$\frac{2}{URF_{\text{source terms}}} \tag{2}$$

for small URFs. Increasing the numerator of this expression from 2 to 3 had negligible impact on the predicted transport variables and outlet particle sizes. Convergence was determined based on mass, momentum and energy residuals below 1×10^{-5} at the end of

each continuous phase update. Decreasing this convergence criterion by an order of magnitude and increasing the number of continuous phase iterations by a factor of two had a negligible impact on the results.

Previous studies have successfully resolved two-way coupled heat and mass transport using the fully polydisperse distribution of various aerosols from experiments (Longest and Hindle 2010; Longest and Hindle 2012; Longest et al., 2011). In this study, the MMAD from the experiments was used to define the mean initial aerosol size. This mean initial aerosol size together with the measured nebulizer liquid output rate, were used to estimate the aerosol number concentrations reported in Table 1. For each model, 3,000 particles with the mean initial size were simulated to predict the multi-way coupled flow fields and outlet particle diameters. Increasing the initial number of representative droplets by an order of magnitude (but keeping the total liquid mass injection rate constant) had a negligible effect on the results.

3. Results

3.1. Initial Droplet Sizes and Validation of the CFD Model

Experimental results of initial aerosol size and the aerosol size when dried using the mixer with ambient conditions along with CFD predictions of droplet size are displayed in Figure 2. Initial droplet MMADs (and standard deviation; SD) based on measurements at 99% RH for the commercial and lab versions of the Aeroneb nebulizer were 4.69 (0.21) μm and 3.90 (0.02) μm, respectively. These initial sizes were measured at a flow rate of approximately 30 LPM and assumed constant for flow rates of 15 and 5 LPM (Table 1). Aerosol MMADs were then determined following generation into the mixer with drying using ambient air (55% RH and 21 °C) (Fig. 2). The CFD model of evaporation in ambient conditions matched the inlet boundary thermodynamic conditions and assumed a thermally insulated wall with no water on the surface. In all CFD simulations, the model began with the conical exit of the mixer, as shown in Figs. 1b and c. In these validation simulations, an additional length of the delivery line was added to account for residence time in both the mixer and impactor. Results of the CFD model in terms of MMAD are shown to adequately match the experimental data for cases with both minor aerosol evaporation (as with the commercial nebulizer) and full aerosol evaporation (as with the lab nebulizer) for flow rates of 15 and 30 LPM (Fig. 2). Differences between the experimental results and predictions likely arise due to the absence of the mixer in the CFD simulations. Still, the comparison provides confidence that the model is capable of simulating multi-way coupling of a polydisperse hygroscopic aerosol in the corrugated tubular geometry considered.

3.2. Add-On Device Performance

Droplet trajectories colored according to mass mean geometric diameters (d_{geo}) are reported in Figure 3 for the three add-on devices considered at a characteristic flow rate of 15 LPM. Panels in the left and right columns represent the commercial and lab devices, respectively. The aerosol was initialized at the experimentally determined initial MMAD for the commercial and lab nebulizers (Table 1). For the insulated system at 15 LPM (Figs. 3a and b), some evaporation is observed due to the low RH of the inlet air resulting in a size reduction of approximately 1 μm for both nebulizers. However, a submicrometer aerosol was not formed. In contrast, the wire heated case (Figs. 3c and d) produces fully evaporated dry particles at the geometry outlet for both the commercial and lab nebulizers. As a result, it appears that sufficient heat transfer occurs in the geometry such that predictions of Eq. (1) can be used to estimate the required input energy and associated wall heat flux. Similarly, the counter-flow heating system results in significant drying of the aerosol (Figs. 3e and f). The high water mass loading of the commercial device (Table 1) prevents full evaporation at

15 LPM; however, an aerosol with a geometric mean diameter of 1.11 μm is formed (Fig. 3e). Reducing the available water mass with the lab nebulizer, which operates at a lower formulation delivery rate, in the counter-flow system is observed to produce fully dried particles (Fig. 3f).

In comparison with results at 15 LPM, droplet trajectories at 5 LPM in the wire heated design are presented in Figure 4. It was expected that reduced flow would allow longer exposure for aerosol evaporation. However, Figure 4 indicates that at 5 LPM gravity causes the aerosol stream to settle toward the lower portion of the tube. This region of high aerosol concentration reaches saturation preventing further evaporation. The symmetric uniform wall heat input then overheats the air in the top of the tube resulting in natural convection flows that cause some particles to spiral up toward the top of the tube and evaporate. However, overall evaporation is relatively low for the commercial and lab devices with exiting mean diameters of 3.23 and 1.71 μm, respectively.

Outlet mean geometric diameters for all systems considered are presented in Table 2. At 5 LPM, only the lab device with counter-flow heating produces a submicrometer particle. As illustrated in Figure 4, the wire heated device at this flow rate provides sufficient thermal energy to evaporate the aerosol, but does not effectively deliver this heat flux. At 15 LPM, both forms of heating effectively dry the aerosol to submicrometer or near submicrometer size for both nebulizers. Still, there is insufficient vapor capacity in the air volume to produce dried particles with the insulated system. It is not until the flow rate is increased to 30 LPM and the lab nebulizer is used that a dried aerosol is produced for the insulated system. As with the 15 LPM condition, both forms of heating produce dried aerosols at the delivery rate of 30 LPM. It is noted that these CFD estimates of evaporated particle size are intended to be conservative by predicting the maximum possible size based on the assumption of no water uptake at the wall surfaces.

Temperature profiles and mass flow rate-averaged outlet temperatures for the three devices and two nebulizers are reported in Fig. 5 for a characteristic flow rate of 15 LPM. With the insulated system, the actively evaporating droplets and absence of additional heat result in an exit temperature of approximately 7 - 9 °C (Fig. 5a and b). For the heated systems, temperatures begin in the range of 10 °C due to prevalent droplet evaporation. The addition of wall heat then raises the vapor capacity of the air and increases the air temperature as the droplets become smaller and less water mass is evaporated. Exit temperatures for fully dried particles are the highest, which include the wire heated cases (Figs. 5c and d) and the counter-flow heated lab nebulizer (Fig. 5e). It is observed that the wire heated cases can easily exceed an expected safe and comfortable delivery temperature maximum of 45 °C, whereas the counter-flow system is limited to a maximum temperature of the input counter-flow airstream (i.e., 42 °C).

Contours of RH and mass flow rate-averaged exit values for counter-flow heating with the commercial and lab nebulizers at 15 LPM are displayed in Fig. 6, which correspond to temperature field Figures 5e and f. For the commercial device, incomplete evaporation of the aerosol results in high RH values. However, the exiting mass flow rate-averaged RH value (72.2%) is below saturated conditions. The lab device with counter-flow heating, which produces a fully dried aerosol, is observed to have a low exiting RH (27.0%). As a result, it appears difficult to both fully dry the aerosol and provide a warm near saturated airstream.

A significant difference between the wire heated and the counter-flow heated devices was observed when the aerosol was turned off. The absence of aerosol delivery may occur if the nebulizer aerosolizes all of the liquid (runs dry) or if the mesh becomes clogged. Because a

majority of the constant input energy in the wire heated case is used to evaporate the aerosol, based on Eq. (1), adding this heat to the air phase alone produced a large increase in temperature with an exit condition of approximately 65 °C based on CFD simulations (not shown). In contrast, the maximum temperature that could be achieved by the counter-flow system without the aerosol is the heating gas air temperature, which was 42 °C. Therefore, it appears that the counter-flow system provided sufficient heat to evaporate the aerosol when needed, but automatically reduced the heat taken up by the central line when the aerosol was removed such that a safe maximum outlet temperature was maintained.

Mass flow rate-averaged outlet temperature and RH values are reported in Table 3 for all devices, nebulizers, and flow rates considered. A safe and comfortable temperature range of 20 - 45 °C was assumed for comparison with the output temperatures. Similarly, an outlet RH criterion of 40% and above was selected with the intention that the aerosol stream would not dry the airways during NIV and could be effectively combined with ECG delivery. Cases where submicrometer (or near submicrometer) aerosols are achieved based on Table 2 are marked with bold type. For a flow rate of 5 LPM, aerosol accumulation along the lower portion of the tube causes unsafe temperature spikes for the wire heated device. In contrast, outlet temperature is observed to remain below 42 °C for all counter-flow heating systems. Furthermore, all counter-flow heating cases achieve a minimum temperature of approximately 30 °C. Considering RH, the insulated cases all achieve RH values near 100%, as expected. Furthermore, RH is observed to respond inversely with temperature so increases in output temperature produce decreases in output RH, which is expected due to the high dependence of saturation vapor pressure on temperature. The addition of heat and increased temperatures are required to evaporate the aerosol in most cases. Therefore, it appears difficult to produce submicrometer aerosols at temperatures above the inlet stream with RH values near saturation conditions.

3.3. Effect of Curvature

The straight tube configuration considered in this study results in the minimum amount of heat transfer and aerosol evaporation that can be achieved by each system. Effects of tube curvature are illustrated in Fig. 7 for the commercial nebulizer with counter-flow heating based on CFD predictions. Compared with the straight tube case, the curved tube configuration selected increases the exit temperature from 29.2 to 36.7 °C. The associated exiting mean particle size decreases from 1.11 μm with the straight configuration to fully dried 0.43 μm particles with tube curvature. The increased water mass in the air associated with increased drying was offset by increased temperature resulting in a reduction of outlet RH from 72.2% to 48.8% with the curved configuration. Based on these observations, additional evaporation is possible by implementing tube curvature. Furthermore, the outlet diameter results reported for straight tubes are a conservative estimate representing the maximum outlet size (i.e., minimum amount of evaporation). Finally, variations in temperature associated with tube curvature make it even more critical that the maximum outlet temperature is limited, as automatically achieved with the counter-flow tube configuration.

3.4. Formation of Nanoparticles

For systems in which dried submicrometer aerosols were formed, nanoparticles ($d_{geo} < 100$ nm) can be achieved by simply decreasing the initial concentration of drug solute in the formulation. Changes in temperature and relative humidity in these systems for the formation of nanoparticles can be neglected because of the small amount of water mass that is vaporized in going from the submicrometer size range to nanoparticles. Considering an initial mass fraction of drug in the nebulized solution, $Y_{initial}$, the fully dried final geometric particle diameter (d_{final}) is predicted as

$$d_{\text{final}} = d_{\text{initial}} \left(Y_{\text{initial}} \frac{\rho_{\text{initial}}}{\rho_{\text{final}}} \right)^{1/3} \quad (3)$$

where ρ represents initial and final density of the droplet or particle. Unfortunately, Eq. (3) reveals that large reductions in the solution concentration, and associated mass of delivered drug for a set time, are required to reduce droplet size to the nanoscale. Writing Eq. (3) in terms of the required mass fraction to reach a target final diameter results in

$$Y_{\text{initial}} = \frac{\rho_{\text{final}}}{\rho_{\text{initial}}} \left(\frac{d_{\text{final}}}{d_{\text{initial}}} \right)^3 \quad (4)$$

In these expressions, the mass fraction of drug ($Y_{initial}$) can be converted to an initial w/v $\left(\bar{\rho}_{\text{initial}}\right)$ typically used in preparing formulations as

$$\bar{\rho}_{\text{initial}} = Y_{\text{initial}} \cdot \rho_{\text{initial}} \quad (5)$$

where the density is entered in g/cm^3 and is initially assumed to be 1 g/cm^3 in this study due to the very low solute concentration values.

To verify that the current systems can produce nanoparticles by reducing the drug concentration in the aqueous formulation, a CFD simulation was conducted for the lab nebulizer with counter-flow heating operating at an aerosol delivery rate of 15 LPM. To produce a target aerosol size of 50 nm, Eq. (4) indicates that the initial mass fraction of drug in the aqueous solution is 2.82×10^{-6} for the lab nebulizer (or 2.82×10^{-4} % w/v). The multi-way coupled CFD solution indicated that the exiting particles were fully dried with a geometric diameter of 50.4 nm. Small differences between the target and exit size exist due to rounding. For the nanoparticle generation system, exiting aerosol stream temperature and RH were within 1 °C and 1% RH of the submicrometer conditions displayed in Figs. 5 and 6. Considering that all cases producing fully dried submicrometer particles had exit RH values well below 100%, it is concluded that these cases can be implemented to form dried nanoparticles of predetermined sizes by reducing the solution concentration based on Eqs. (3) - (5).

3.5. Verification of CFD Results with Experiments

To verify the CFD predictions, an experimental study was performed using the counter-flow device with the lab nebulizer and flow rates of 5 and 15 LPM. These two cases were selected for verification based on their ability to effectively form a submicrometer aerosol. In the experiments, the device was allowed to reach steady state conditions over a period of 5 minutes prior to sizing the aerosol. Following aerosol generation, the aerosol was sampled into the cascade impactor using the counter-flow add-on device. The mean MMADs exiting the counter-flow device at flow rates of 5 and 15 LPM were 0.79 (SD = 0.11) μm and 0.48 (SD = 0.06) μm, respectively. Assuming an initially monodisperse aerosol from the nebulizer, density estimates of the exiting droplets for the 5 and 15 LPM cases were 1.032 and 1.170 g/cm^3, resulting in exiting geometric droplet diameters of 0.78 and 0.44 μm, respectively. Figure 8 compares these estimated geometric diameters with the CFD predictions reported in Table 2 for the counter-flow device and lab nebulizer. As observed in the figure, the CFD estimates are in generally good agreement with the experimental predictions in term of both trend and value. Differences between the experimental results and model predictions likely arise due to the approximation of a monodisperse aerosol, some

deposition that may occur in the aerosol mixer, and small curvatures occurring with the counter-flow line in the experimental setup.

4. Discussion

In conclusion, results of this study indicate that simple add-on devices can be coupled with conventional mesh nebulizers to form directly inhalable submicrometer and nanoparticle aerosols for improved respiratory drug delivery. Through appropriate selection of flow rates and nebulizers, which define the initial aerosol size and number concentration, submicrometer aerosols were formed with the three devices considered. Use of conventional mesh nebulizers to form the aerosol allows these devices to be easily reproduced and cost effective. High delivery rates of drug are achieved by starting with large nebulized droplets and then forming the submicrometer or nanometer aerosol using evaporation. Results of the current study show that the submicrometer and nanometer aerosols are formed in an airstream that can be directly inhaled at a safe and comfortable temperature and relative humidity. Direct inhalation of the aerosol avoids the need for collection of the particles and re-aerosolization, which is often difficult due to significant inter-particle cohesion forces (Chan 2006; Chan and Kwok 2011). Compared with single nozzle electrospray (Fu et al., 2011; Ijsebaert et al., 2001), the current device delivers the solution formulation at a liquid flow rate that is at least an order of magnitude higher and avoids droplet charge, which can cause unwanted deposition in the delivery system and extrathoracic airways. As with CAG (Hindle et al., 2004; Longest et al., 2007), the approach considered in this study allows some control over outlet temperature and relative humidity. In general, the temperature is controlled by the amount of thermal energy absorbed by the aerosol stream. For a wall vapor neutral system, the relative humidity adjusts based on the temperature and amount of water mass in the droplets. As a result, it was not possible to achieve a combination of a submicrometer aerosol at a temperature above body conditions and near saturated RH. Therefore, delivery with ECG will still required a separate saturated vapor line and use of a dual flow mouthpiece (Hindle and Longest 2010). However, the proposed device may be ideal for EEG based delivery, which relies on the natural water vapor in the airways to foster growth. Furthermore, the proposed devices will provide a readily available source of inhalable nanometer particles for directly testing the effectiveness of nanoaerosol pharmaceutical delivery, although the delivered doses may require prolonged administration times.

A primary contribution of this study is the comparison of wire and counter-flow heating for producing a directly inhalable submicrometer aerosol from commercial nebulizers. Conditioning of respiratory gasses typically employs wire heating with the heating element either inside the delivery line or embedded in the tube wall (Rea et al., 2010). Co-flow or jacketed heating with water has also recently been proposed for conditioning respiratory gases delivered during high flow oxygen or blended oxygen delivery (Guerrero et al., 2003). However, these systems have never been used to produce submicrometer aerosol for direct inhalation. Based on results of this study, wire heating appears unsafe for producing a directly inhaled submicrometer aerosol. The wire delivers a nearly constant heat flux with sufficient energy to both heat the airstream and evaporate the liquid droplets. As indicated in Eq. (1), the heat required to vaporize the aerosol is significantly greater than the heat required to warm the airstream. When the aerosol delivery is suspended or if the aerosol is not uniformly distributed in the tube cross section, excessive and uncontrolled heating of the air occurs. In contrast, the counter-flow design was found to provide sufficient energy to produce the desired submicrometer aerosol and avoided overheating the airstream. Based on the counter-flow design, the amount of energy input into the aerosol stream varies with air temperature such that the aerosol exit temperature never exceeds the heating inlet temperature of 42 °C. Overheating with the wire-based case could be limited by the

inclusion of a temperature sensor and an electronic feedback control loop. However, both the sensor and temperature controller will increase the cost and complexity of the wire design and could fail, creating unsafe conditions. In contrast, the counter-flow design has a self adjusting temperature control mechanism based on the physics of heat transfer. Moreover, the proposed air-jacketed heating can be operated with the same gas source used for aerosol delivery and is much simpler than current water jacketed systems used with gas delivery.

The mesh nebulizers considered in this study have liquid delivery rates of 0.4 and 0.2 ml/min (Table 1). For a typical nebulizer solution volume of 4 ml, delivery requires 10 or 20 minutes, which is consistent with current clinical nebulizer applications. The drug concentration employed for the submicrometer aerosols generated in this study was 0.1% w/v, which would result in a 4 mg (or 4000 μg) nominal drug dose. Typically, drug doses delivered with nebulizers are significantly larger than with handheld dry powder inhalers (DPIs) and metered dose inhalers (MDIs). This is because of the poor delivery performance of most nebulizers. With ECG or EEG delivery, lung deposition fractions of the nebulized dose are expected to be on the order of 100% (Hindle and Longest 2010; Longest et al., 2011; Tian et al., 2011), if breath actuation of the nebulizer is employed. As a result, the proposed system is capable of delivering 4000 μg to the lungs over a period of 10 - 20 minutes, depending on the nebulizer selected (Aeroneb Pro vs. Lab). For typical DPIs and MDIs as well as new softmist inhalers, the nominal dose of bronchodilators or corticosteroids is in the range of 50 - 250 μg (depending on the drug), with approximately 30-90% loss in the oropharyngeal region (Longest and Hindle 2009; Longest et al., 2012; Newman and Busse 2002; Zhang et al., 2007b). Therefore, typical lung doses of these medications can be as low as 5-75 μg. In contrast, inhaled antibiotics frequently require nominal doses of 35 mg to be effective (Geller et al., 2002) due to the similar low deposition efficiency. Therefore, using the proposed system, comparable lung doses of bronchodilators and corticosteroids or other high potency drugs delivered by DPIs and MDIs could be achieved with a very quick administration time. Delivery of inhaled antibiotics could also be practical by maximizing the drug concentration in the solution while maintaining submicrometer inhaled size, based on Eq. (3), considering the improved efficiency of EEG and ECG delivery. In contrast, reducing the initial concentration of drug to 2.82×10^{-4} % w/v in order to produce 50 nm particles reduces the nominal dose in a 4 ml solution to 11.3 μg. This value is within the therapeutically effective range for bronchodilators and corticosteroids in adults assuming complete delivery (as described above). It may also be appropriate for the delivery of these and other low dose medications to infants and children (Fink 2004; Rubin 2011). However, nanoparticle delivery of high dose medicines like inhaled antibiotics and surfactants does not appear feasible over conventional short administration times (10-20 mins). As a result, ECG and EEG approaches with submicrometer aerosols that are capable of delivering on the order of 10 mg of drug over typical nebulization times may be superior for many medications compared with envisioned nanoparticle delivery. Potentially more effective methods to generate submicrometer aerosols using solution-based MDIs (Stein and Myrdal 2004) and DPIs are currently under investigation.

In conclusion, the mesh nebulizers selected were shown to effectively produce submicrometer aerosols when coupled with a mixer and three add-on devices. Counter-flow heating was the preferred method of producing the submicrometer aerosol based on the heat transfer effectiveness and control of outlet thermodynamic conditions. Optimal conditions for ECG and EEG drug delivery were identified for different routes of inhalation. Future work is needed to explore the performance of other nebulizers, which may better provide a submicrometer or nanoparticle aerosol without heating, and to evaluate the deposition of the generated submicrometer aerosols in patient interface devices such as nasal cannula and

masks. Development of a delivery system capable of generating submicrometer aerosols in a saturated warm airstream would also be advantageous.

Acknowledgments

This study was supported by Award Numbers R01 HL107333 and R21 HL094991 from the National Heart, Lung, And Blood Institute. The content is solely the responsibility of the authors and does not necessarily represent the official views of the National Heart, Lung, And Blood Institute or the National Institutes of Health.

ABBREVIATIONS

ACI	Andersen cascade impactor
AS	albuterol sulfate
CFD	computational fluid dynamics
DPI	dry powder inhaler
ECG	enhanced condensational growth
EEG	enhanced excipient growth
HPLC	high-performance liquid chromatography
LPM	liters per minute
LRN	Low Reynolds number
MDI	metered dose inhaler
MMAD	mass median aerodynamic diameters
MOUDI	micro-orifice uniform deposition impactor
NIV	non-invasive ventilation
RH	relative humidity
SD	standard deviation
SPAG	small particle aerosol generator

References

Abdelrahim ME, Chrystyn H. Aerodynamic characteristics of nebulized terbutaline sulphate using the next generation impactor (NGI) and CEN method. Journal of Aerosol Medicine and Pulmonary Drug Delivery. 2009; 22(1):19–28. [PubMed: 19392586]

Abdelrahim ME, Plant PK, Chrystyn H. The relative lung and systemic bioavailability of terbutaline following nebulisation in non-invasively ventilated patients. International Journal of Pharmaceutics. 2011; 420(2):313–318. [PubMed: 21944891]

Ari A, Harwood R, Sheard M, Dailey P, Fink JB. In Vitro Comparison of Heliox and Oxygen in Aerosol Delivery Using Pediatric High Flow Nasal Cannula. Pediatric Pulmonology. 2011; 46(8): 795–801. [PubMed: 21438178]

Asgharian B, Price OT. Deposition of ultrafine (Nano) particles in the human lung. Inhalation Toxicology. 2007; 19:1045–1054. [PubMed: 17957545]

Azarmi S, Roa WH, Lobenberg R. Targeted delivery of nanoparticles for the treatment of lung diseases. Advanced Drug Delivery Reviews. 2008; 60:863–875. [PubMed: 18308418]

Chan H-K. Dry powder aerosol drug delivery - Opportunities for colloid and surface scientists. Colloids and Surfaces A: Physicochem. Eng. Aspects. 2006; 284-285:50–55.

Chan HK, Kwok PCL. Production methods for nanodrug particles using the bottom-up approach. Advanced Drug Delivery Reviews. 2011; 63(6):406–416. [PubMed: 21457742]

Chen X, Young TJ, Sarkari M, Williams RO, Johnston KP. Preparation of cyclosporine A nanoparticls by evaporative precipitation into aqueous solution. International Journal of Pharmaceutics. 2002; 242:3–14. [PubMed: 12176220]

Cheng KH, Cheng YS, Yeh HC, Guilmette RA, Simpson SQ, Yang SQ, Swift DL. In vivo measurements of nasal airway dimensions and ultrafine aerosol depositing in human nasal and oral airways. Journal of Aerosol Science. 1996; 27:785–801.

Couvreur P, Dubernet C, Puisieux F. Controlled Drug-Delivery With Nanoparticles - Current Possibilities And Future-Trends. European Journal Of Pharmaceutics And Biopharmaceutics. 1995; 41(1):2–13.

Dandekar P, Venkataraman C, Mehra A. Pulmonary Targeting of Nanoparticle Drug Matrices. Journal Of Aerosol Medicine And Pulmonary Drug Delivery. 2010; 23(6):343–353. [PubMed: 20455773]

Dhand R. Nebulizers that use a vibrating mesh or plate with multiple apertures to generate aerosol. Respiratory Care. 2002; 47(12):1406–1416. [PubMed: 12467499]

Dhand R. Inhalation therapy in invasive and noninvasive mechanical ventilation. Current Opinion in Critical Care. 2007; 13:27–38. [PubMed: 17198046]

Dhand R. Aerosol delivery during mechanical ventilation: From basic techniques to new devices. Journal of Aerosol Medicine and Pulmonary Drug Delivery. 2008; 21(1):45–60. [PubMed: 18518831]

El-Gendy N, Gorman EM, Munson EJ, Berkland C. Budesonide Nanoparticle Agglomerates as Dry Powder Aerosols With Rapid Dissolution. Journal Of Pharmaceutical Sciences. 2009; 98(8):2731–2746. [PubMed: 19130469]

Fink JB. Aerosol delivery to ventilated infant and pediatric patients. Respiratory Care. 2004; 49(6): 653–665. [PubMed: 15165300]

Finlay, WH. The Mechanics of Inhaled Pharmaceutical Aerosols. Academic Press; San Diego: 2001.

Fu HJ, Patel AC, Holtzman MJ, Chen DR. A new electrospray aerosol generator with high particle transmission efficiency. Aerosol Science And Technology. 2011; 45(10):1176–1183.

Geller DE, Pitlick WH, Nardella PA, Tracewell WG, Ramsey BW. Pharmacokinetics and bioavailability of aerosolized tobramycine in cyctic fibrosis. Chest. 2002; 122:219–226. [PubMed: 12114362]

Green, DW. Perry's Chemical Engineers' Handbook. McGraw-Hill; New York: 1997.

Guerrero ML, Cuneo BM, Hnatiuk OW, Shorr A. Vapotherm: A novel high-flow oxygen delivery system. Chest. 2003; 124(4):93S–93S.

Hindle, M.; Gupta, R.; Cox, KA. Adding pharmaceutical flexibility to the capillary aerosol generator. In: Dalby, RN.; Byron, PR.; Peart, J.; Suman, JD.; Farr, SJ., editors. Respiratory Drug Delivery IX. DHI Publishing; River Grove, IL: 2004. p. 247-254.

Hindle M, Longest PW. Evaluation of enhanced condensational growth (ECG) for controlled respiratory drug delivery in a mouth-throat and upper tracheobronchial model. Pharmaceutical Research. 2010; 27:1800–1811. [PubMed: 20454837]

Hindle M, Longest PW. Condensational growth of combination drug-excipient submicrometer particles for targeted high efficiency pulmonary delivery: Evaluation of formulation and delivery device. Journal of Pharmacy and Pharmacology. 2012 In press.

Ijsebaert JC, Geerse KB, Marijnissen JCM, Lammers J-WJ, Zanen P. Electro-hydrodynamic atomization of drug solutions for inhalation purposes. Journal of Applied Physiology. 2001; 91:2735–2741. [PubMed: 11717241]

Jaques PA, Kim CS. Measurement of total lung deposition of inhaled ultrafine particles in healthy men and women. Inhalation Toxicology. 2000; 12(8):715–731. [PubMed: 10880153]

Kays, WM.; Crawford, ME. Convective Heat and Mass Transfer. McGraw-Hill; New York: 1993.

Kuhli M, Weiss M, Steckel H. A sampling and dilution system for droplet aerosols from medical nebulisers developed for use with an optical particle counter. Aerosol Science. 2009; 40:523–533.

Lai SK, Wang Y-Y, Hanes J. Mucus-penetrating nanoparticles for drug and gene delivery to mucosal tissues. Advanced Drug Delivery Reviews. 2009; 61:158–171. [PubMed: 19133304]

Longest PW, Hindle M. Evaluation of the Respimat Soft Mist inhaler using a concurrent CFD and in vitro approach. Journal of Aerosol Medicine and Pulmonary Drug Delivery. 2009; 22(2):99–112. [PubMed: 18956950]

Longest PW, Hindle M. CFD simulations of enhanced condensational growth (ECG) applied to respiratory drug delivery with comparisons to in vitro data. Journal of Aerosol Science. 2010; 41:805–820. [PubMed: 20835406]

Longest PW, Hindle M. Numerical model to characterize the size increase of combination drug and hygroscopic excipient nanoparticle aerosols. Aerosol Science and Technology. 2011; 45:884–899. [PubMed: 21804683]

Longest PW, Hindle M. Condensational growth of combination drug-excipient submicrometer particles: Comparison of CFD predictions with experimental results. Pharmaceutical Research. 2012; 29:707–721. [PubMed: 21948458]

Longest PW, Hindle M, Das Choudhuri S, Byron PR. Numerical simulations of capillary aerosol generation: CFD model development and comparisons with experimental data. Aerosol Science and Technology. 2007; 41:952–973.

Longest PW, McLeskey JT, Hindle M. Characterization of nanoaerosol size change during enhanced condensational growth. Aerosol Science and Technology. 2010; 44:473–483. [PubMed: 20640054]

Longest PW, Tian G, Hindle M. Improving the lung delivery of nasally administered aerosols during noninvasive ventilation - An application of enhanced condensational growth (ECG). Journal of Aerosol Medicine and Pulmonary Drug Delivery. 2011; 24(2):103–118. DOI: 10.1089/jamp.2010.0849. [PubMed: 21410327]

Longest PW, Tian G, Walenga RL, Hindle M. Comparing MDI and DPI aerosol deposition using in vitro experiments and a new stochastic individual path (SIP) model of the conducting airways. Pharmaceutical Research. 2012 DOI: 10.1007/s11095-012-0691-y.

Longest PW, Vinchurkar S. Validating CFD predictions of respiratory aerosol deposition: effects of upstream transition and turbulence. Journal of Biomechanics. 2007; 40:305–316. [PubMed: 16533511]

Longest PW, Xi J. Effectiveness of direct Lagrangian tracking models for simulating nanoparticle deposition in the upper airways. Aerosol Science and Technology. 2007; 41:380–397.

Longest PW, Xi J. Condensational growth may contribute to the enhanced deposition of cigarette smoke particles in the upper respiratory tract. Aerosol Science and Technology. 2008; 42:579–602.

Martonen TB. Mathematical model for the selective deposition of inhaled pharmaceuticals. Journal of Pharmaceutical Sciences. 1993; 82(12):1191–1199. [PubMed: 8308694]

Newman SP, Busse WW. Evolution of dry powder inhaler design, formulation, and performance. Respiratory Medicine. 2002; 96:293–304. [PubMed: 12113378]

Nikander K, Prince I, Coughlin S, Warren S, Taylor G. Mode of Breathing-Tidal or slow and deep-through the I-neb adaptive delivery (ADD) system affects lung deposition of 99mTc-DTPA. Journal of Aerosol Medicine. 2010; 23(S1):S37–S43.

Pitance L, Vecellio L, Leal T, Reychler G, Reychler H, Liistro G. Delivery Efficacy of a Vibrating Mesh Nebulizer and a Jet Nebulizer under Different Configurations. Journal Of Aerosol Medicine And Pulmonary Drug Delivery. 2010; 23(6):389–396. [PubMed: 20958144]

Rea H, McAuley S, Jayaram L, Garrett J, Hockey H, Storey L, O'Donnell G, Haru L, Payton M, O'Donnell K. The clinical utility of long-term humidification therapy in chronic airway disease. Respiratory Medicine. 2010; 104:525–533. [PubMed: 20144858]

Rubin BK. Pediatric aerosol therapy: New devices and new drugs. Respiratory Care. 2011; 56(9): 1411–1421. [PubMed: 21944688]

Skaria S, Smaldone GC. Omron NE U22: Comparison Between Vibrating Mesh and Jet Nebulizer. Journal Of Aerosol Medicine And Pulmonary Drug Delivery. 2010; 23(3):173–180. [PubMed: 20500093]

Stein SW, Myrdal PB. A theoretical and experimental analysis of formulation and device parameters affecting solution MDI size distributions. Journal of Pharmaceutical Sciences. 2004; 93:2158–2175. [PubMed: 15236462]

Tian G, Longest PW, Su G, Hindle M. Characterization of respiratory drug delivery with enhanced condensational growth (ECG) using an individual path model of the entire tracheobronchial airways. Annals of Biomedical Engineering. 2011; 39(3):1136–1153. [PubMed: 21152983]

Vinchurkar S, Longest PW. Evaluation of hexahedral, prismatic and hybrid mesh styles for simulating respiratory aerosol dynamics. Computers and Fluids. 2008; 37:317–331.

Wilcox, DC. Turbulence Modeling for CFD. 2nd Ed. DCW Industries, Inc.; California: 1998.

Xi J, Longest PW. Transport and deposition of micro-aerosols in realistic and simplified models of the oral airway. Annals of Biomedical Engineering. 2007; 35(4):560–581. [PubMed: 17237991]

Xi J, Longest PW. Effects of oral airway geometry characteristics on the diffusional deposition of inhaled nanoparticles. ASME Journal of Biomechanical Engineering. 2008a; 130:011008.

Xi J, Longest PW. Numerical predictions of submicrometer aerosol deposition in the nasal cavity using a novel drift flux approach. International Journal Of Heat And Mass Transfer. 2008b; 51:5562–5577.

Yang JZ, Young AL, Chiang PC, Thurston A, Pretzer DK. Fluticasone and budesonide nanosuspensions for pulmonary delivery: preparation, characterization, and pharmacokinetic studies. Journal of Pharmaceutical Sciences. 2008; 97:4869–4878. [PubMed: 18351635]

Yurteri CU, Hartman RPA, Marijnissen JCM. Producing pharmaceutical particles via electrospraying with an emphasis on nano and nano structured particles - A review. KONA Powder and Particle Journal. 2010; 28:91–115.

Zhang G, David A, Wiedmann TS. Performance of the vibrating membrane aerosol generation device: Aeroneb micropump nebulizer. Journal of Aerosol Medicine. 2007a; 20(4):408–416. [PubMed: 18158713]

Zhang Y, Gilbertson K, Finlay WH. In vivo-in vitro comparison of deposition in three mouth-throat models with Qvar and Turbuhaler inhalers. Journal of Aerosol Medicine. 2007b; 20(3):227–235. [PubMed: 17894531]

- Submicrometer and nanometer particles from mesh nebulizers with add-on devices
- Experimental determination of initial aerosol size and evaporated size
- Wire heated design produced excessive heating of the aerosol stream in some cases
- Counter-flow heating produced dried particles with a limit to maximum temperature
- Outlet temperatures with counter-flow design are safe for direct inhalation

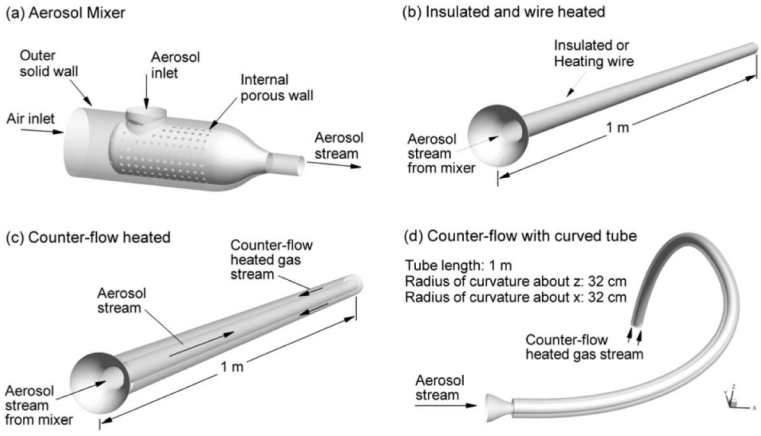

Figure 1.

Devices used to produce submicrometer and nanometer aerosols from conventional mesh nebulizers including the (a) custom aerosol mixer (or diluter) for combining the inlet gas with the nebulized droplets, (b) insulated and wire heated 12 mm diameter tubes, (c) counter-flow configuration with a jacket of heated air, and (d) curved counter-flow heated model.

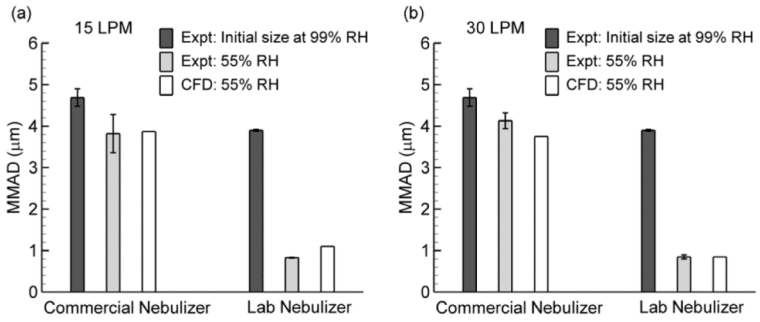

Figure 2.

Experimentally determined initial aerosol mass median aerodynamic diameter (MMAD) based on sampling at 99% relative humidity (RH) and amount of aerosol evaporation in ambient air (55% RH) based on experiments and CFD simulations for the commercial and lab nebulizers at sampling gas flow rates of (a) 15 and (b) 30 LPM. Agreement between the experimental values of evaporated aerosol size and CFD predictions help to verify that the model is accurately predicting thermodynamic conditions, multi-way coupling between the phases, and droplet size.

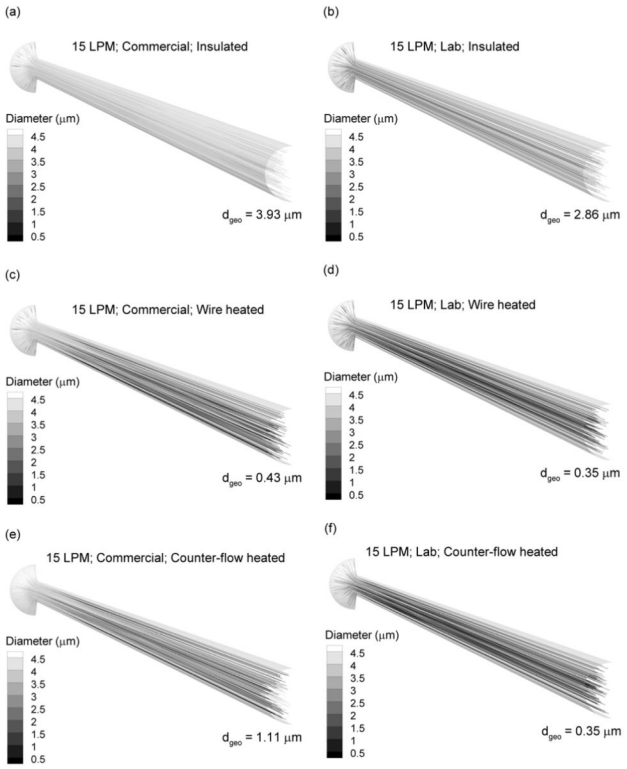

Figure 3.
Droplet trajectories colored according to geometric diameter and outlet mass mean geometric diameters at 15 LPM for the (a and b) insulated line, (c and d) wire heated design, and (e and f) co-flow heated design. Panels in the left and right columns are for the commercial and lab nebulizers, respectively. At 15 LPM, all heated designs produce submicrometer or nearly submicrometer particles.

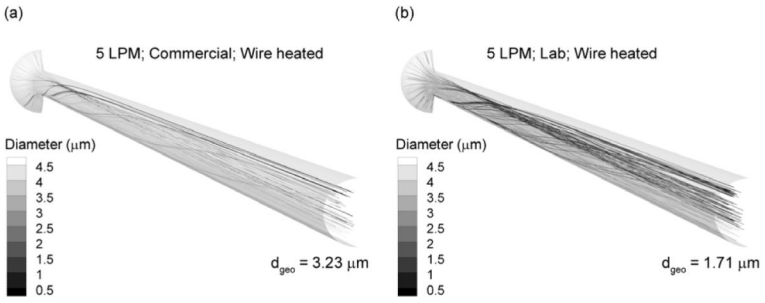

Figure 4.

Droplet trajectories colored according to geometric diameter at a flow rate of 5 LPM for the (a) commercial and (b) lab nebulizers. Gravitational settling at 5 LPM results in a non-uniform concentration of particles in the tube cross section. Uniform heat flux on the surface produces ineffective heat transfer to this region of concentrated aerosol, reduced evaporation, and overheating of the airstream.

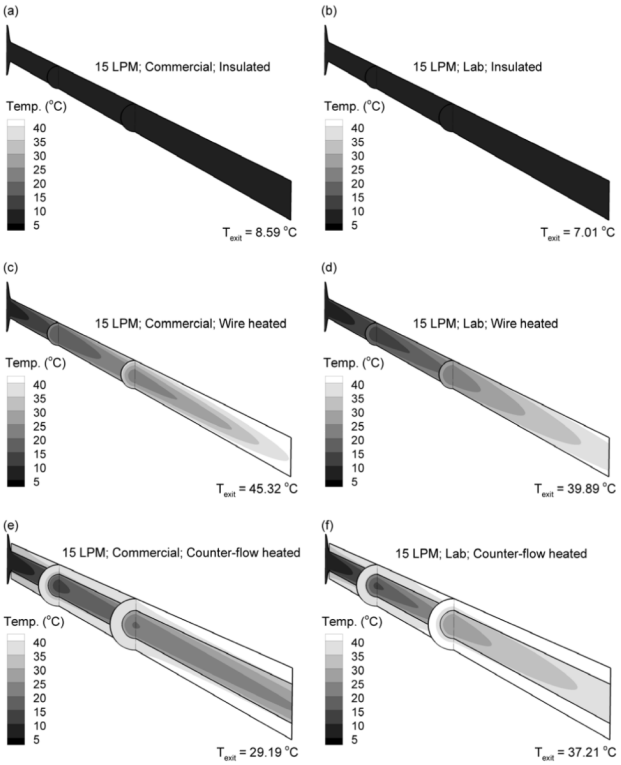

Figure 5.
Temperature profiles and mass flow rate-averaged outlet temperatures at 15 LPM for the (a and b) insulated line, (c and d) wire heated design, and (e and f) co-flow heated design. Panels in the left and right columns are for the commercial and lab nebulizers, respectively.

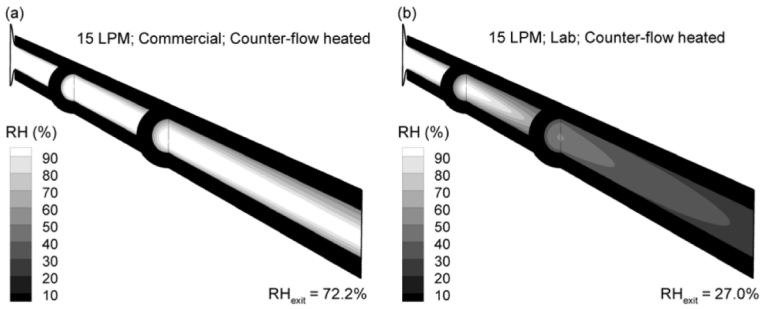

Figure 6.
Relative humidity profiles and mass flow rate-averaged outlet RH values at 15 LPM for the (a) commercial vs. (b) lab nebulizers.

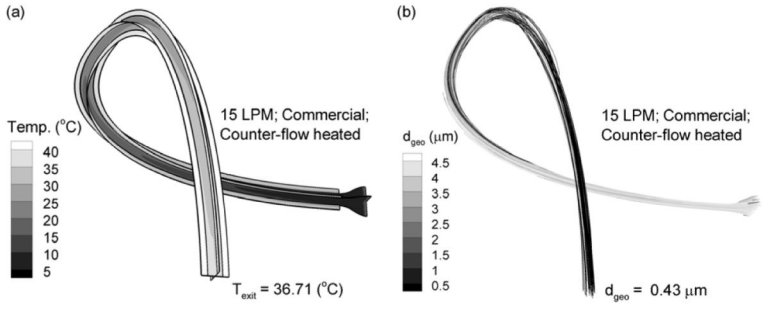

Figure 7.
Effects of tube curvature for an aerosol stream temperature of 15 LPM, the commercial nebulizer, and counter-flow heating in terms of (a) temperature profiles and (b) aerosol size.

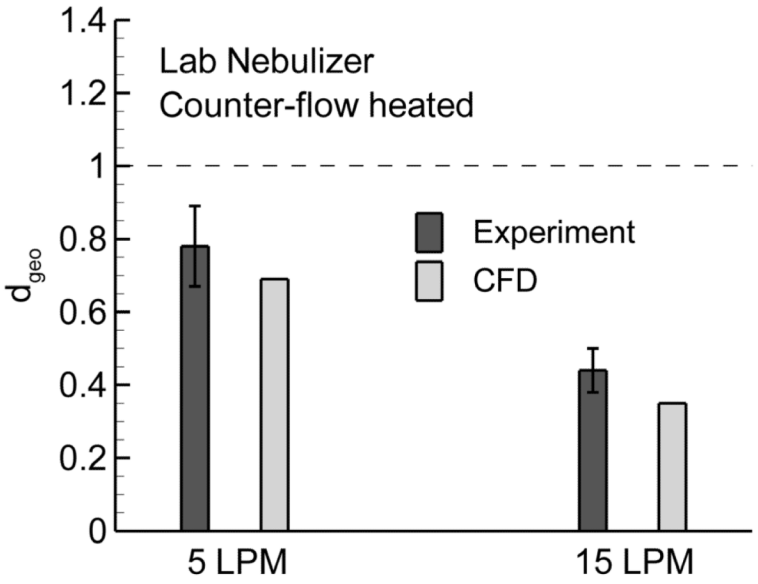

Figure 8.
Comparison of outlet mean geometric diameter between experimental results and model predictions using the counter-flow device and lab nebulizer at flow rates of 5 and 15 LPM. The error bars represent +/− one standard deviation of the experimental data. The CFD predictions are in general agreement with the experimental results.

Table 1

Properties of the commercial (Pro) and lab versions of the AeroNeb nebulizer.

Air Flow Rate [LPM]	**5**	**15**	**30**
Commercial Nebulizer			
Q_{liquid} [ml/min][a]	0.4	0.4	0.4
$\dot{m}_{liquid}$ [g/s][a]	6.67×10^{-3}	6.67×10^{-3}	6.67×10^{-3}
MMAD (SD) [μm][a]	4.69 (0.21)	4.69 (0.21)	4.69 (0.21)
n [part/cm^3][b]	1.48×10^6	4.94×10^5	2.47×10^5
Lab Nebulizer			
Q_{liquid} [ml/min][a]	0.2	0.2	0.2
$\dot{m}_{liquid}$ [g/s][a]	3.33×10^{-3}	3.33×10^{-3}	3.33×10^{-3}
MMAD (SD) [μm][a]	3.90 (0.02)	3.90 (0.02)	3.90 (0.02)
n [part/cm^3][b]	1.28×10^6	4.28×10^5	2.14×10^5

[a]Measured

[b]Calculated based on the assumption of a monodisperse aerosol

Table 2

Outlet geometric diameters (d_{geo}) in micrometers for the commercial (Pro) and lab Aeroneb nebulizers and three wall conditions.

	Commercial Nebulizer			Lab Nebulizer		
	5 LPM	**15 LPM**	**30 LPM**	**5 LPM**	**15 LPM**	**30 LPM**
Insulated	4.04	3.93	3.66	3.94	2.86	0.35
Wall heated	3.23	0.43	0.43	1.71	0.35	0.35
Counterflow heated	2.40	1.11	0.43	0.69	0.35	0.35

Table 3

Temperature (T) and Relative Humidity (RH) for the commercial (Pro) and lab Aeroneb nebulizers and three wall conditions.

	Commercial Nebulizer						Lab Nebulizer					
	5 LPM		15 LPM		30 LPM		5 LPM		15 LPM		30 LPM	
	T (°C)	RH (%)	T (°C)	RH (%)	T (°C)	RH (%)	T (°C)	RH (%)	T (°C)	RH (%)	T (°C)	RH (%)
Insulated	8.6	98.7	7.5	96.7	7.0	98.6	7.8	100.0	7.0	99.3	8.0	84.2
Wall heated	136.9	1.5	**45.3**	**34.0**	**40.1**	**23.0**	65.1	16.1	**39.9**	**23.1**	**37.7**	**13.7**
Counterflow heated	40.0	48.3	29.2[a]	72.2[a]	**28.9**	**39.9**	**38.7**	**52.1**	**37.2**	**27.0**	**32.9**	**17.7**

Bold values represent conditions producing submicrometer particles based on Table 2.

[a]Produced a near submicrometer size of 1.11 μm.